

Stripe quadrupole order in the nematic phase of $\text{FeSe}_{1-x}\text{S}_x$

W.-L. Zhang,^{1,*} S.-F. Wu,^{1,†} S. Kasahara,² T. Shibauchi,³ Y. Matsuda,² and G. Blumberg^{1,4,‡}

¹Department of Physics & Astronomy, Rutgers University, Piscataway, New Jersey 08854, USA

²Department of Physics, Kyoto University, Kyoto, 606-8502, Japan

³Department of Advanced Materials Science, University of Tokyo, Kashiwa, Chiba 277-8561, Japan

⁴National Institute of Chemical Physics and Biophysics, Akadeemia tee 23, 12618 Tallinn, Estonia

(Dated: May 17, 2018)

We use polarization-resolved electronic Raman spectroscopy to study charge dynamics in non-magnetic $\text{FeSe}_{1-x}\text{S}_x$ superconductor. We observe two features of the XY quadrupole symmetry: a low-energy quasi-elastic peak (QEP) and an electronic continuum. The QEP exhibits critical enhancement upon cooling towards the structural transition at $T_S(x)$. Below $T_S(x)$, the QEP diminishes gradually, and a gap with temperature evolution reminiscent of a mean-field order parameter opens in the continuum. The intensity of the QEP develops with increasing sulfur doping x and maximizes at $x \approx 0.15$, while the gap magnitude decreases with the suppression of $T_S(x)$. We interpret the development of the gap in the quadrupole scattering channel as the formation of a stripe quadrupole order: a wave of quadrupole moment without charge or spin modulation.

The iron-based superconductors (FeSCs) exhibit a complex phase diagram with multiple competing orders. For most of the FeSCs, an electronic nematic phase transition takes place at T_S , which is closely followed by a magnetic phase transition at T_N [1–4]. Superconductivity emerges in close proximity to the electronic nematic and the antiferromagnetic orders. The highest superconducting (SC) transition temperature T_C often occurs when the nematic and the magnetic orders are fully suppressed but the orbital/charge or spin fluctuations remain strong [5–8]. The relationship between these fluctuations and superconductivity has been a focus of intense research [4, 9–15].

FeSe crystals provide the simplest case to elucidate the relationship between the orbital/multipolar charge order and superconductivity because it shows nematicity in the absence of magnetic order [9, 18, 19]. At ambient pressure, a structural phase transition that breaks the four-fold rotational symmetry (C_4) takes place at $T_S = 90$ K. Strong electronic quadrupole fluctuations involving the charge transfer between the degenerate $\text{Fe } 3d_{xz}$ and $3d_{yz}$ orbitals, which contribute to most of the electronic density of states near E_F , have been observed above T_S [20–23]. The degeneracy of the d_{xz} and d_{yz} orbitals is lifted in the broken symmetry phase [24–26], where although the lattice is only weakly distorted, prominent anisotropy is found for electronic properties [16, 27, 28]. For crystals, superconductivity emerges in the nematic phase at $T_C \approx 9$ K [18], while for FeSe monolayer films deposited on SrTiO_3 substrate, T_C can be enhanced for almost an order of magnitude [29–31]. Orbital-selective SC pairing has been reported by ARPES and quasiparticle interference (QPI) in bulk FeSe: the SC gap energy is large only for specific region of the nematic Fermi surfaces with the d_{yz} orbital characters [16, 27, 28]. However, the mechanism behind the puzzling orbital-selective superconductivity has not been discussed in depth.

In this Letter, we employ polarization-resolved Raman

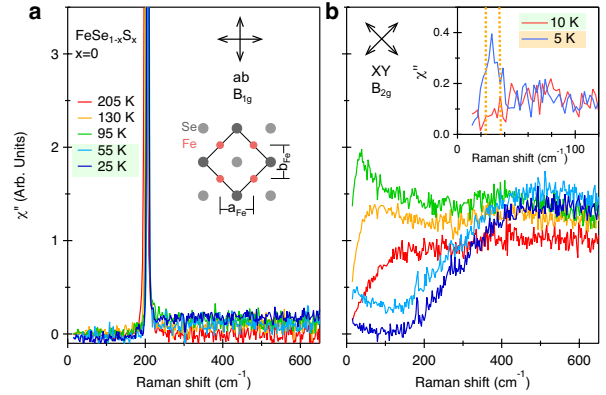


FIG. 1. Temperature evolution of the $B_{1g}(ab)$ and $B_{2g}(XY)$ symmetry Raman response $\chi''(\omega, T)$ for pristine FeSe. Inset of (a) shows the top view of the FeSe layer. Dark and light gray circles represent the Se above and below the Fe layer. The 2-Fe unit cell for the high-temperature phase is shown by solid lines. In the low-temperature phase, the nearest Fe-Fe bonding distance a_{Fe} becomes larger than b_{Fe} while a_{Fe} and b_{Fe} remain orthogonal. Inset of (b): $\chi''(\omega, T)$ in the XY symmetry channel of FeSe in the normal state (10 K) and SC state (5 K). The magnitude of the two superconducting gaps $2\Delta_{SC} = 3$ and 4.6 meV measured by tunneling spectroscopy are shown with the vertical dotted lines [16, 17].

spectroscopy to study charge quadrupole dynamics in non-magnetic superconductor $\text{FeSe}_{1-x}\text{S}_x$ [20, 32]. We observe two main features in the XY symmetry scattering channel: (i) a low-energy quasi-elastic peak (QEP) and (ii) a high-energy electronic continuum extending beyond 2000 cm^{-1} with a peak at 450 cm^{-1} . Above $T_S(x)$, the QEP exhibits enhancement and softening upon cooling in wide temperature and the sulfur doping range with a quantum critical scaling for critical doping at $x_{cr} \approx 0.15$. While the QEP and the broad spectral feature around 450 cm^{-1} for pristine FeSe has been reported in Refs. [22, 23, 33], here we demonstrate that be-

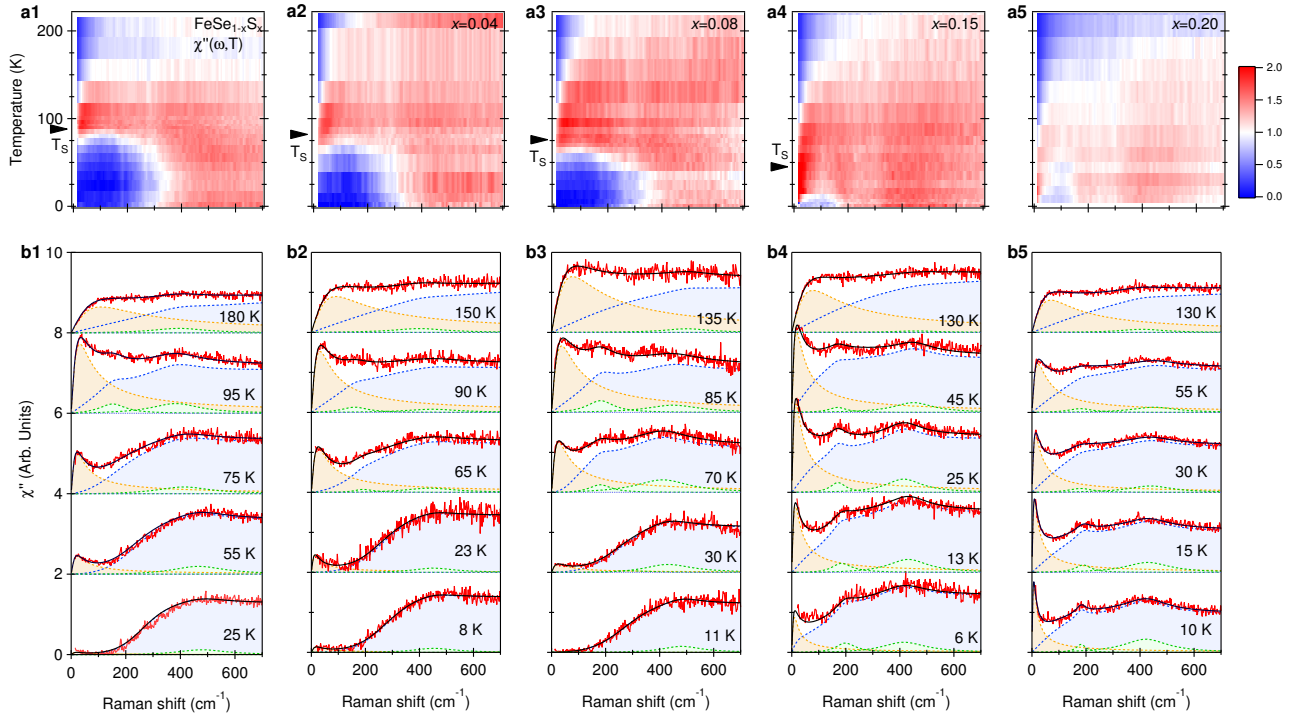


FIG. 2. (a1-a5) Temperature evolution of the XY symmetry Raman susceptibility $\chi''(\omega, T)$ for $\text{FeSe}_{1-x}\text{S}_x$ ($x = 0, 0.04, 0.08, 0.15$ and 0.2). Arrows at the temperature axis denote $T_S(x)$. (b1-b5) $\chi''(\omega, T)$ (red) at representative temperatures and their fits (black) with the decompositions of the QEP χ''_{QEP} (orange shade) and the continuum $\chi''_C \times \Theta$ (blue shade). The two Lorentz oscillators χ''_L at around 190 and 450 cm^{-1} are shown in green shade.

low $T_S(x)$ an unexpected gap gradually develops in the electronic continuum for system with gapless Fermi surface. The temperature dependence of the gap $2\Delta_x(T)$ scales with the orthorhombic order parameter and the gap magnitude is proportional to $T_S(x)$ with the ratio $2\Delta_x(0)/k_B T_S(x) = 4.8$. In the study of $\text{FeSe}_{1-x}\text{S}_x$ phase diagram, we demonstrate that the continuum is due to quadrupole fluctuations with staggered moments and the the gap formation below $T_S(x)$ is due to long-range stripe quadrupole (SQ) order. The latter also provides natural explanations for the observed phenomena of orbital-selective superconductivity.

$\text{FeSe}_{1-x}\text{S}_x$ ($x = 0, 0.04, 0.08, 0.15$ and 0.2) single crystals were grown by chemical vapor transport technique as described in [20]. Substitution of sulfur for selenium acts as negative pressure, which suppresses T_S while the system remains non-magnetic, and superconductivity remains robust [20, 28, 32]. Strain-free crystals were cleaved in nitrogen atmosphere and positioned in a continuous flow optical cryostat. Polarization-resolved Raman spectra were acquired in a quasi-backscattering geometry from the ab surface. We used 2.6 eV excitation from a Kr^+ laser. The laser power was kept below 10 mW for most measurements and less than 2 mW for the measurements in the superconducting state. The laser heating $\approx 1\text{ K/mW}$ was estimated by the appear-

ance of the stripe pattern on the crystal surface at T_S [34]. The Raman scattering signal was analyzed by a custom triple-grating spectrometer and the data were corrected for the spectral response of the spectrometer.

Figs. 1(a-b) show the temperature dependence of the Raman response for the pristine FeSe in the B_{1g} (ab) and B_{2g} (XY) symmetry channels (D_{4h} point group) defined for the 2-Fe unit cell. B_{1g} channel contains the Fe phonon mode ($\approx 195\text{ cm}^{-1}$) [33] above a weak temperature independent continuum background (Fig. 1a). In contrast, the electronic Raman continuum in the B_{2g}

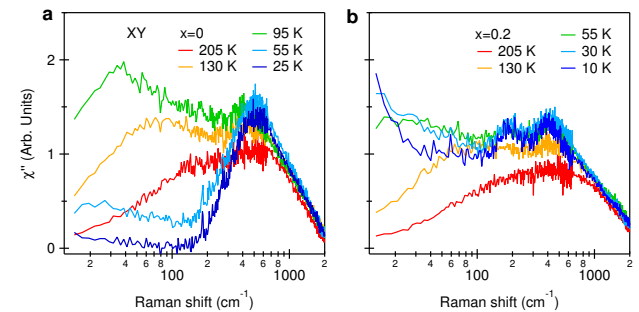


FIG. 3. Temperature evolution of the XY symmetry Raman response $\chi''(\omega, T)$ for (a) FeSe and (b) $\text{FeSe}_{0.8}\text{S}_{0.2}$.

channel (Fig. 1b) is strong; it is composed of several spectral features with remarkable temperature dependence:

(i) *A low-energy quasi-elastic scattering peak (QEP).* The intensity of the QEP is weak at high temperatures. Upon cooling, it softens, gains intensity, reaches its maximum intensity just above T_S , and then gradually loses its intensity below T_S (Fig. 2b1). In the superconducting phase, the QEP acquires coherence and undergoes a metamorphosis into a coherent in-gap collective mode, similar to other FeSCs [36–40] (inset Fig. 1b).

(ii) *A broad electronic continuum* extending beyond 2000 cm^{-1} with a peak at 450 cm^{-1} . The intensity of this continuum increases with cooling and then saturates at low temperature (Fig. 3a). Below T_S , a significant gap suppression develops at 400 cm^{-1} .

In Figs. 2 and 3, we show temperature evolution of the XY Raman response in $\text{FeSe}_{1-x}\text{S}_x$. The 450 cm^{-1} peak appears at low temperature for all sulfur contents in both the tetragonal and orthorhombic phase (Fig. 3). Hence, this broad feature is not exclusive for the nematic phase [41]. An additional weak peak at 190 cm^{-1} appears for samples with sulfur doping. At the lowest temperature, a full gap suppression is observed for all doping concentrations except for $x = 0.15$, where a reduced scattering intensity remains in the gap. For $x = 0.2$, which remains tetragonal in whole temperature range, no gap suppression is observed.

We perform a multi-component fit to the XY symmetry Raman response (Figs. 2b1-b5). Here we represent QEP as a Drude function $\chi''_{QEP}(\omega, T) = A_{QEP}^2 \omega \Gamma_{QEP}/(\omega^2 + \Gamma_{QEP}^2)$ and the electronic continuum as $\chi''_C(\omega, T) = A_C^2 \tanh[\omega/\Gamma_C] + \chi''_L(\omega, T)$, where $\chi''_L(\omega, T)$ are two Lorentz oscillators around 190 and 450 cm^{-1} . $\Gamma_C(T)$ follows a quadratic temperature dependence for all samples except for composition in the vicinity of the critical doping $x \approx 0.17$ [20], where its temperature dependence is nearly linear [17]. Below $T_S(x)$, the gap-like suppression is modeled by $\Theta(\omega, T) = \frac{1}{2}(1 + \tanh[\frac{\omega - 2\Delta(T)}{2k_B T_{eff}}])$, where $2\Delta(T)$ is the gap energy and T_{eff} is an effective temperature. By applying the gap function independently to the QEP or the continuum spectral components, we find that only the latter is consistent with the data. Thus, the QEP and the broad continuum arise from distinct fluctuations, and the gap only opens in the continuum component.

The reduced gap energy $2\Delta_x(T)/k_B T_S(x)$ collapses to a universal temperature dependence with $2\Delta_x(0)/k_B T_S(x) = 4.8$ (Fig. 4a). The temperature dependence of $2\Delta_x(T)$ follows the lattice order parameter $\delta(T) = (a + b)/(a - b)$ [35], manifesting direct connection between formation of the gap and the lattice orthorhombicity.

We calculate the static Raman susceptibility for the QEP and the continuum contributions, $\chi_{QEP}(0, T)$ and $\chi_C(0, T)$, by Kramers-Kronig transformation [17]. In

contrast to the mild temperature evolution of $\chi_C(0, T)$, a critical enhancement is seen above $T_S(x)$ for $\chi_{QEP}(0, T)$ (Figs. 4b1-b5). This suggests that there are two types of quadrupole fluctuations in the tetragonal phase. The temperature dependence of the QEP is generic for most FeSCs [5, 22, 34, 38, 42]. It was related to the ferro-quadrupole (FQ) fluctuations of a d -wave Pomeranchuk instability at $q=0$. Locally, the charge transfer between the nearly degenerate d_{xz} and d_{yz} orbitals creates a charge quadrupole with moment proportional to the local charge imbalance $Q \propto n_{d_{xz}} - n_{d_{yz}}$ [12, 38, 42–47]. In Fig. 5b we illustrate a snapshot of the FQ fluctuations. Such excitation results in a $\Gamma_4^+(B_{2g})$ symmetry dynamic deformation of the Fermi surface pockets with nodal lines in the X/Y directions. We fit $\chi_{QEP}(0, T > T_S)$ with a Curie-Weiss function $\chi_{QEP}(0, T) \propto Q^2(x)/(T - T_0(x))$ (Fig. 4c1-c5), where $T_0(x)$ is the Weiss temperature [5, 38].

In Fig. 5a we display the fitting parameters $Q(x)$, $2\Delta_x(0)$ and $T_0(x)$ together with the $\text{FeSe}_{1-x}\text{S}_x$ phase diagram. $T_0(x)$ is tens of K below T_S , decreases with x and vanishes at $x \approx 0.15$, close to the nematic quantum critical point (QCP) as it was also reported by the elastoresistence study [20]. $Q(x)$ increases with x and maximizes at $x \approx 0.15$, while $2\Delta_x(0)$ decreases with x .

Now we turn to the origin of the gap. Such gap cannot be described by non-interacting electron-hole excitations because the Fermi surface pockets remain gapless [24–26, 48]. Appearance of the gap only in the XY symmetry channel implies a density wave in either a_{Fe} or b_{Fe} direction. Because neither charge nor spin modulation in the nematic phase was detected [18], the possibilities of charge/spin density wave gap are ruled out.

We propose a collinear stripe d_{xz}/d_{yz} quadrupole order consisting of staggered Q and $-Q$ quadrupole moments, as depicted in Fig. 5c. The order parameter in real space can be defined as $\phi_{XY} = \prod_{r=A \text{ site}} |Q_r\rangle \times \prod_{r=B \text{ site}} |Q_r\rangle$, which would give rise to the XY symmetry gap. Here $Q/-Q$ quadrupole moments reside on iron sites $r = A/B$.

We note that a FQ order may also open an Ising nematic gap in the XY spectra. The gap energy would correspond to the barrier for flipping the nematic order parameter. However, the ARPES data and RG calculations show that the order parameter involving the d_{xz} and d_{yz} orbitals at Γ and M_X/M_Y points have nearly equivalent magnitude but opposite sign [24–26, 48]. Such nearly equal total occupation of these two orbitals can be realized by the SQ, rather than the FQ order.

XY symmetry Raman scattering directly couples to $\Delta L = 2$ quadrupole excitations, making it a unique tool to probe the SQ order parameter or its dynamical fluctuations. In contrast, given that the total charge on each Fe site $n_r = n_{r,d_{xz}} + n_{r,d_{yz}}$ is preserved, the charge sensitive probes such as scanning tunneling spectroscopy, X-ray diffraction or optical conductivity are unresponsive to such SQ order. We also notice that neutron scatter-

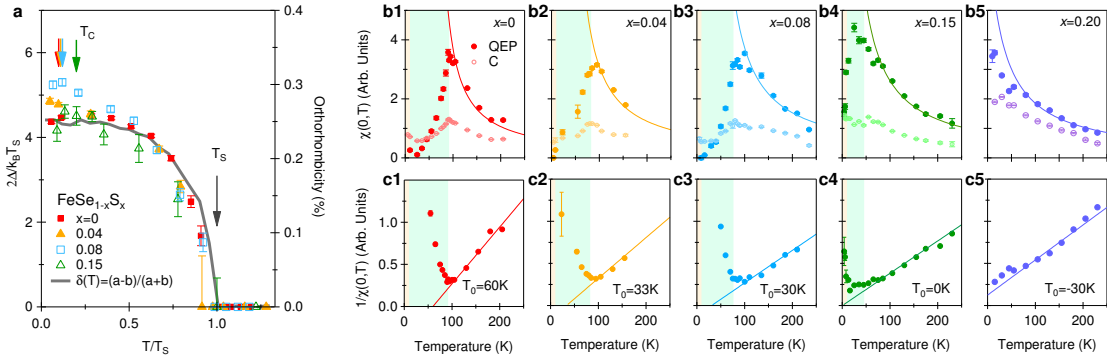


FIG. 4. (a) Temperature and doping evolution of the nematic gap $2\Delta(T)/k_B T_S$ in $\text{FeSe}_{1-x}\text{S}_x$ as a function of the reduced temperature T/T_S . The gray curve is the lattice order parameter $\delta(T) = (a-b)/(a+b)$ for FeSe from ref [35]. T_S and T_C are denoted by arrows. (b1-b5) Static Raman susceptibility $\chi_{QEP}(0, T)$ and $\chi_C(0, T)$ for $x = 0, 0.04, 0.08, 0.15$ and 0.2 . Curie-Weiss fit for $\chi_{QEP}(0, T)$ at $T > T_S$ is shown by the solid curve. The yellow and cyan shades indicate $T_C(x)$ and $T_S(x)$, respectively. (c1-c5) Temperature dependence of the inverse static susceptibility $1/\chi_{QEP}(0, T)$ and the Weiss temperature $T_0(x)$. Error bars are the fitting standard errors.

ing works suggest a hidden collinear antiferromagnetic quadrupole (AFQ) order for in FeSe [49, 50]. If the magnetic AFQ is at the same ordering vector as the charge SQ, a bilinear coupling between these two orders is allowed.

In the SQ-ordered phase, if the translational symmetry is broken and d_{xz}/d_{yz} orbital-density wave forms, the quasi-particle weight Z_{xz} in the d_{xz} orbitals would be suppressed. The reduction of Z_{xz} would naturally result in a smaller SC gap for the d_{xz} orbitals [51] and overall in suppression of T_C , consistent with the observation of *orbital-dependent superconducting gap* reported by ARPES and QPI [16, 27]. On the other hand, due to the coupling to the substrate, the SQ fluctuations are expected to be removed for the high- T_C monolayer FeSe films deposited on the SrTiO_3 , resulting in a high- T_C phenomenon [29, 30, 52].

In summary, we use polarization-resolved Raman spectroscopy to study the evolution of charge dynamics in nonmagnetic $\text{FeSe}_{1-x}\text{S}_x$ superconductor as a function of sulfur doping and temperature at above and below $T_S(x)$. We observe the development of a QEP on cooling towards $T_S(x)$ and a pronounced gap in the XY symmetry continuum below $T_S(x)$. By increasing sulfur concentration, the QEP intensity is enhanced, while the gap magnitude and $T_S(x)$ decrease. The ferro-quadrupole fluctuations are strongest in the vicinity of the nematic critical point at $x_{cr} \approx 0.15$. The appearance of robust low-energy gap implies the formation of a long-range quadrupole order, for example, a staggered stripe order. In the presence of the SQ order, the superconductivity on the d_{xz} orbital is suppressed due to the reduction of the quasi-particle weight along the SQ ordering vector direction, which provides a natural explanation for the observed orbital-selective superconductivity in bulk FeSe [16, 27] as well as for the phenomena of high- T_C superconductiv-

ity in monolayer FeSe films [29, 30] where the SQ order is expected to be suppressed due to the coupling to the substrate.

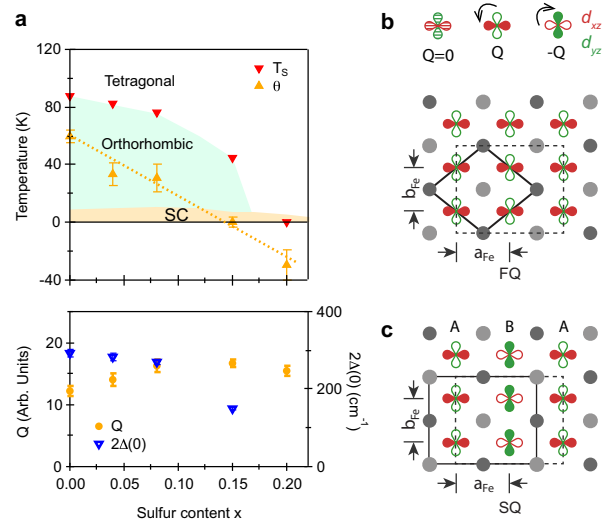


FIG. 5. (a) Phase diagram and the fitting parameters in $\text{FeSe}_{1-x}\text{S}_x$. The FQ moment $Q(x)$ (empty squares, lower panel) and the Weiss temperature $T_0(x)$ (upward triangles, upper panel) are obtained from the Curie-Weiss fit of $\chi_{QEP}(0, T)$. $\Delta_x(0)$ (downward triangles, lower panel) is obtained from $\Delta_x(T)$. (b) A snapshot of the B_{2g} symmetry FQ fluctuations consist of d_{xz}/d_{yz} charge quadrupoles from the top view of a FeSe layer. An elementary quadrupole Q moment is created by on-site charge transfer from d_{yz} to d_{xz} orbital while a quadrupole moment $-Q$ is created by charge transfer from d_{xz} to d_{yz} orbital. (c) SQ ground state with staggered $|Q\rangle$ (A site) and $|-Q\rangle$ (B site) in vertical stripes. $a_{Fe} > b_{Fe}$. Solid lines in (b) and (c) show the quadrupole primitive cell and the dashed lines show the unit cell for FQ and SQ state, respectively.

The work at Rutgers was supported by the U.S. Department of Energy, Office of Basic Energy Sciences, Division of Materials Sciences and Engineering under Contract No. DE-SC0005463. The work in Japan was supported by Grant-in-Aids for Scientific Research (Proposals No. 15H02106, 15H03688, and 25220710), and by Grant-in-Aids on Innovative Areas “Topological Materials Science” (No. 15H05852), from Japan Society for the Promotion of Science (JSPS). GB acknowledges the hospitality of the Aspen Center for Physics, which is supported by NSF grant PHY-1607611.

-
- * wz131@physics.rutgers.edu
- † On leave from Beijing National Laboratory for Condensed Matter Physics and Institute of Physics, Chinese Academy of Sciences, Beijing, 100190, China
- ‡ girsh@physics.rutgers.edu
- [1] E. Fradkin, S. A. Kivelson, M. J. Lawler, J. P. Eisenstein, and A. P. Mackenzie, *Annu. Rev. Condens. Matter Phys.* **1**, 153 (2010).
- [2] G. R. Stewart, *Nat. Phys.* **83**, 1589 (2011).
- [3] J. Paglione and R. L. Greene, *Nat Phys.* **6**, 645 (2010).
- [4] R. M. Fernandes, A. V. Chubukov, and J. Schmalian, *Nat. Phys.* **10**, 97 (2014).
- [5] Y. Gallais, R. M. Fernandes, I. Paul, L. Chauvière, Y.-X. Yang, M.-A. Méasson, M. Cazayous, A. Sacuto, D. Colson, and A. Forget, *Phys. Rev. Lett.* **111**, 267001 (2013).
- [6] A. E. Bohmer, P. Burger, F. Hardy, T. Wolf, P. Schweiss, R. Fromknecht, M. Reinecker, W. Schranz, and C. Meingast, *Phys. Rev. Lett.* **112**, 047001 (2014).
- [7] J.-H. Chu, H.-H. Kuo, J. G. Analytis, and I. R. Fisher, *Science* **337**, 710 (2012).
- [8] X. Lu, J. T. Park, R. Zhang, H. Luo, A. H. Nevidomskyy, Q. Si, and P. Dai, *Science* **345**, 657 (2014).
- [9] S.-H. Baek, D. V. Efremov, J. M. Ok, J. S. Kim, J. van den Brink, and B. Büchner, *Nat Mater.* (2014).
- [10] A. E. Böhmer and C. Meingast, *Comptes Rendus Physique*, (2015).
- [11] A. V. Chubukov, M. Khodas, and R. M. Fernandes, *Phys. Rev. X* **6**, 041045 (2016).
- [12] Y. Gallais and I. Paul, *Comptes Rendus Physique* **17**, 113 (2016).
- [13] A. P. Dioguardi, T. Kissikov, C. H. Lin, K. R. Shirer, M. M. Lawson, H.-J. Grafe, J.-H. Chu, I. R. Fisher, R. M. Fernandes, and N. J. Curro, *Phys. Rev. Lett.* **116**, 107202 (2016).
- [14] Y. Schattner, S. Lederer, S. A. Kivelson, and E. Berg, *Phys. Rev. X* **6**, 031028 (2016).
- [15] L. Classen, R.-Q. Xing, M. Khodas, and A. V. Chubukov, *Phys. Rev. Lett.* **118**, 037001 (2017), and refs therein.
- [16] P. O. Sprau, A. Kostin, A. Kreisel, A. E. Böhmer, V. Taufour, P. C. Canfield, S. Mukherjee, P. J. Hirschfeld, B. M. Andersen, and J. C. S. Davis, *Science* **357**, 75 (2017).
- [17] See Supplemental Material at [url put by publisher] for details of data analysis, phonons and the spectra in the superconducting state, which includes Refs. [53–59].
- [18] T. M. McQueen, A. J. Williams, P. W. Stephens, J. Tao, Y. Zhu, V. Ksenofontov, F. Casper, C. Felser, and R. J. Cava, *Phys. Rev. Lett.* **103**, 057002 (2009).
- [19] A. E. Böhmer, T. Arai, F. Hardy, T. Hattori, T. Iye, T. Wolf, H. v. Löhneysen, K. Ishida, and C. Meingast, *Phys. Rev. Lett.* **114**, 027001 (2015).
- [20] S. Hosoi, K. Matsuura, K. Ishida, H. Wang, Y. Mizukami, T. Watashige, S. Kasahara, Y. Matsuda, and T. Shibauchi, *Proc. Natl. Acad. Sci. USA* **113**, 8139 (2016).
- [21] M. A. Tanatar, A. E. Böhmer, E. I. Timmons, M. Schütt, G. Drachuck, V. Taufour, K. Kothapalli, A. Kreyssig, S. L. Bud'ko, P. C. Canfield, R. M. Fernandes, and R. Prozorov, *Phys. Rev. Lett.* **117**, 127001 (2016).
- [22] P. Massat, D. Farina, I. Paul, S. Karlsson, P. Strobel, P. Toulemonde, M.-A. Masson, M. Cazayous, A. Sacuto, S. Kasahara, T. Shibauchi, Y. Matsuda, and Y. Gallais, *Proc. Natl. Acad. Sci. USA* **113**, 9177 (2016).
- [23] A. Baum, H. N. Ruiz, N. Lazarević, Y. Wang, T. Böhm, R. Hosseiniyan Ahangharnejhad, P. Adelmann, T. Wolf, Z. V. Popović, B. Moritz, T. P. Devereaux, and R. Hackl, ArXiv e-prints (2017), [arXiv:1709.08998](https://arxiv.org/abs/1709.08998).
- [24] M. D. Watson, T. K. Kim, L. C. Rhodes, M. Eschrig, M. Hoesch, A. A. Haghhighirad, and A. I. Coldea, *Phys. Rev. B* **94**, 201107 (2016).
- [25] A. I. Coldea and M. D. Watson, *Annu. Rev. Condens. Matter Phys.* **9**, 125 (2018).
- [26] A. Fedorov, A. Yaresko, T. K. Kim, Y. Kushnirenko, E. Haubold, T. Wolf, M. Hoesch, A. Grüneis, B. Büchner, and S. V. Borisenko, *Sci. Rep.* **6**, 36834 (2016).
- [27] H. C. Xu, X. H. Niu, D. F. Xu, J. Jiang, Q. Yao, Q. Y. Chen, Q. Song, M. Abdel-Hafiez, D. A. Chareev, A. N. Vasiliev, Q. S. Wang, H. L. Wo, J. Zhao, R. Peng, and D. L. Feng, *Phys. Rev. Lett.* **117**, 157003 (2016).
- [28] T. Hanaguri, K. Iwaya, Y. Kohsaka, T. Machida, T. Watashige, S. Kasahara, T. Shibauchi, and Y. Matsuda, ArXiv e-prints (2017), [arXiv:1710.02276](https://arxiv.org/abs/1710.02276).
- [29] W. Qing-Yan, L. Zhi, Z. Wen-Hao, Z. Zuo-Cheng, Z. Jin-Song, L. Wei, D. Hao, O. Yun-Bo, D. Peng, C. Kai, W. Jing, S. Can-Li, H. Ke, J. Jin-Feng, J. Shuai-Hua, W. Ya-Yu, W. Li-Li, C. Xi, M. Xu-Cun, and X. Qi-Kun, *Chin. Phys. Lett.* **29**, 037402 (2012).
- [30] J.-F. Ge, Z.-L. Liu, C. Liu, C.-L. Gao, D. Qian, Q.-K. Xue, Y. Liu, and J.-F. Jia, *Nat Mater.* **14**, 285 (2015).
- [31] D.-H. Lee, *Science* **357**, 32 (2017).
- [32] K. Matsuura, Y. Mizukami, Y. Arai, Y. Sugimura, N. Maejima, A. Machida, T. Watanuki, T. Fukuda, T. Yajima, Z. Hiroi, K. Y. Yip, Y. C. Chan, Q. Niu, S. Hosoi, K. Ishida, K. Mukasa, T. Watashige, S. Kasahara, J.-G. Cheng, S. K. Goh, Y. Matsuda, Y. Uwatoko, and T. Shibauchi, (2017), [arXiv:1704.02057](https://arxiv.org/abs/1704.02057).
- [33] V. Gnezdilov, Y. G. Pashkevich, P. Lemmens, D. Wulferding, T. Shevtsova, A. Gusev, D. Chareev, and A. Vasiliev, *Phys. Rev. B* **87**, 144508 (2013).
- [34] F. Kretzschmar, T. Bohm, U. Karahasanoğlu, B. Muschler, A. Baum, D. Jost, J. Schmalian, S. Caprara, M. Grilli, C. Di Castro, J. G. Analytis, J. H. Chu, I. R. Fisher, and R. Hackl, *Nat. Phys.* **12**, 560 (2016).
- [35] Q. Wang, Y. Shen, B. Pan, Y. Hao, M. Ma, F. Zhou, P. Steffens, K. Schmalzl, T. R. Forrest, M. Abdel-Hafiez, X. Chen, D. A. Chareev, A. N. Vasiliev, P. Bourges, Y. Sidis, H. Cao, and J. Zhao, *Nat. Mater.* **15**, 159 (2016).
- [36] F. Kretzschmar, B. Muschler, T. Böhm, A. Baum, R. Hackl, H.-H. Wen, V. Tsurkan, J. Deisenhofer, and A. Loidl, *Phys. Rev. Lett.* **110**, 187002 (2013).
- [37] A. Hinojosa, J. Cai, and A. V. Chubukov, *Phys. Rev. B*

- [93](#), 075106 (2016).
- [38] V. K. Thorsmølle, M. Khodas, Z. P. Yin, C. Zhang, S. V. Carr, P. Dai, and G. Blumberg, [Phys. Rev. B](#) **93**, 054515 (2016).
- [39] Y. Gallais, I. Paul, L. Chauvière, and J. Schmalian, [Phys. Rev. Lett.](#) **116**, 017001 (2016).
- [40] S.-F. Wu, P. Richard, H. Ding, H.-H. Wen, G. Tan, M. Wang, C. Zhang, P. Dai, and G. Blumberg, [Phys. Rev. B](#) **95**, 085125 (2017).
- [41] This is in contrast to interpretations in Ref. [22, 23], where authors claimed a relation between the 450 cm^{-1} peak to nematicity, see [17] for details.
- [42] W.-L. Zhang, P. Richard, H. Ding, A. S. Sefat, J. Gillett, S. E. Sebastian, M. Khodas, and G. Blumberg, ArXiv e-prints (2014), [arXiv:1410.6452](#).
- [43] C.-C. Lee, W.-G. Yin, and W. Ku, [Phys. Rev. Lett.](#) **103**, 267001 (2009).
- [44] W. Lv, J. Wu, and P. Phillips, [Phys. Rev. B](#) **80**, 224506 (2009).
- [45] T. Saito, S. Onari, and H. Kontani, [Phys. Rev. B](#) **82**, 144510 (2010).
- [46] H. Yamase and R. Zeyher, [Phys. Rev. B](#) **88**, 125120 (2013).
- [47] H. Kontani and Y. Yamakawa, [Phys. Rev. Lett.](#) **113**, 047001 (2014).
- [48] R.-Q. Xing, L. Classen, M. Khodas, and A. V. Chubukov, [Phys. Rev. B](#) **95**, 085108 (2017).
- [49] R. Yu and Q. Si, [Phys. Rev. Lett.](#) **115**, 116401 (2015).
- [50] Q. Wang, Y. Shen, B. Pan, X. Zhang, K. Ikeuchi, K. Iida, A. D. Christianson, H. C. Walker, D. T. Adroja, M. Abdel-Hafez, X. Chen, D. A. Chareev, A. N. Vasiliev, and J. Zhao, [Nat. Commun.](#) **7**, 12182 (2016).
- [51] A. Kreisel, B. M. Andersen, P. O. Sprau, A. Kostin, J. C. S. Davis, and P. J. Hirschfeld, [Phys. Rev. B](#) **95**, 174504 (2017).
- [52] P. Zhang, X.-L. Peng, T. Qian, P. Richard, X. Shi, J.-Z. Ma, B. B. Fu, Y.-L. Guo, Z. Q. Han, S. C. Wang, L. L. Wang, Q.-K. Xue, J. P. Hu, Y.-J. Sun, and H. Ding, [Phys. Rev. B](#) **94**, 104510 (2016).
- [53] V. Cvetkovic and O. Vafek, [Phys. Rev. B](#) **88**, 134510 (2013).
- [54] J. Hu and N. Hao, [Phys. Rev. X](#) **2**, 021009 (2012).
- [55] W.-L. Zhang, W. R. Meier, T. Kong, P. C. Canfield, and G. Blumberg, ArXiv e-prints (2018), [arXiv:1804.06963](#).
- [56] Y. A. Pomeranchuk, [Sov. Phys. JETP](#) **8**, 361 (1958).
- [57] M. Khodas, A. V. Chubukov, and G. Blumberg, [Phys. Rev. B](#) **89**, 245134 (2014).
- [58] S. Maiti, A. V. Chubukov, and P. J. Hirschfeld, [Phys. Rev. B](#) **96**, 014503 (2017).
- [59] S.-F. Wu, W.-L. Zhang, L. Li, H.-B. Cao, H.-H. Kung, A. S. Sefat, H. Ding, P. Richard, and G. Blumberg, ArXiv e-prints (2017), [arXiv:1712.01903](#).

SUPPLEMENTAL MATERIALS

Background subtraction

The imaginary part of the Raman susceptibility $\chi''_{\mu\nu}(\omega, T)$ is calculated from the total secondary emission intensity $I_{\mu\nu}(\omega, T) = [1 + n(\omega, T)]\chi''_{\mu\nu}(\omega, T) + I_{lumi}$, where $\mu(\nu)$ denotes the polarization of the incident and scattered light, $[1 + n(\omega, T)] = [1 - \exp(-\hbar\omega/k_B T)]^{-1}$ is the Bose distribution function for Stokes Raman scattering and I_{lumi} is the luminescence background. The scattering intensity has been corrected for the system response and normalized by the incident laser power and the acquisition time.

Raman scattering spectra were acquired in three polarization configurations ($\mu\nu = XY$, ab and aa) to separate excitations in distinct symmetry channels ($B_{1g} = ab$, $B_{2g} = XY$, and $A_{1g} = aa(bb) - XY$). In Figs. 6a and b we show the secondary emission intensity for the ab and XY geometries at various temperatures for pristine FeSe.

The ab geometry scattering continuum is almost independent of temperature. Therefore, we attribute it to mainly luminescence background. Assuming that the luminescence is unpolarized (same for the ab and XY geometries), we calculate the Raman response in the ab and XY scattering geometries with a temperature independent background estimated from the lowest ab geometry scattering continuum (B_{1g} phonon subtracted), as shown by the grey shade in Figs. 6a and b.

The A_{1g} symmetry scattering intensity is calculated by subtracting the XY symmetry secondary emission intensity from aa , as shown in Figs. 6c and d.

Doping dependence of phonon spectra

We observe two Raman active phonon modes from the ab -surface of pristine FeSe in quasi-back-scattering geometry at room temperature: an A_{1g} phonon at 180 cm^{-1} associated with Se vibrations and a B_{1g} phonon at 195 cm^{-1}

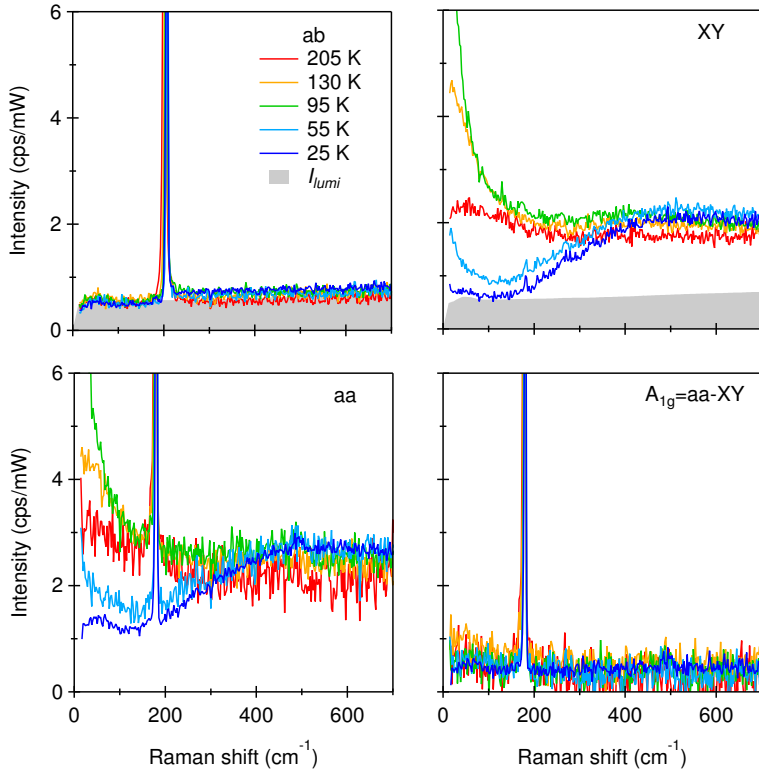


FIG. 6. (a-c) The secondary emission intensity for the ab , XY and aa scattering geometries for pristine FeSe. The luminescence background for the ab and XY scattering geometries is calculated from the emission continuum in the ab geometry. (d) A_{1g} symmetry scattering intensity calculated as the difference between secondary emission intensity in the aa and XY geometries.

associated with Fe vibrations [33]. With sulfur substitution, the energy of the B_{1g} phonon changes only slightly, while the A_{1g} phonon gradually softens and loses intensity. A new A_{1g} phonon mode appears at around 193 cm^{-1} , its intensity increases with sulfur doping x (Fig. 7).

Doping dependence of the 450 cm^{-1} feature

A broad feature peaked at 450 cm^{-1} is observed in the XY symmetry spectra for all studied $\text{FeSe}_{1-x}\text{S}_x$ ($x = 0, \dots, 0.2$) samples. Similar data were reported for pristine FeSe in the prior literatures, however, inconsistent interpretations were offered by different authors: in the Ref. [22] the 450 cm^{-1} feature was interpreted as nematic response of ill-defined quasiparticles in a bad metal, while in Ref. [23] the feature was interpreted as two-magnon excitation whose intensity abruptly increase below T_S .

In Fig.2 (main text) and Fig. 8 we compare temperature evolution of the XY symmetry Raman response for pristine ($x = 0$, $T_S=88\text{ K}$) and heavily sulfur doped ($x = 0.2$, always tetragonal) crystals. The 450 cm^{-1} feature appears for both samples at all measured temperatures, in both tetragonal and orthorhombic phases. More importantly, for each given temperature the feature lineshape is quite similar for both samples: the only distinction between the tetragonal and orthorhombic phases is the gap-like suppression in the broad continuum, which evolves as the nematic order parameter (see also Fig. 9). This implies that sharpening of the 450 cm^{-1} feature upon cooling is just due to temperature effect only. Thus, this feature is not exclusive to the nematic phase. The data we present in Fig. 8 supports neither the quasi-particle nematic response interpretation proposed in the Ref. [22] nor the magnetic scattering interpretation proposed in the Ref. [23]. The broad feature could arise from an interband transition analogously to similar feature present in the spectra for NaFeAs structure discussed in Ref. [38].

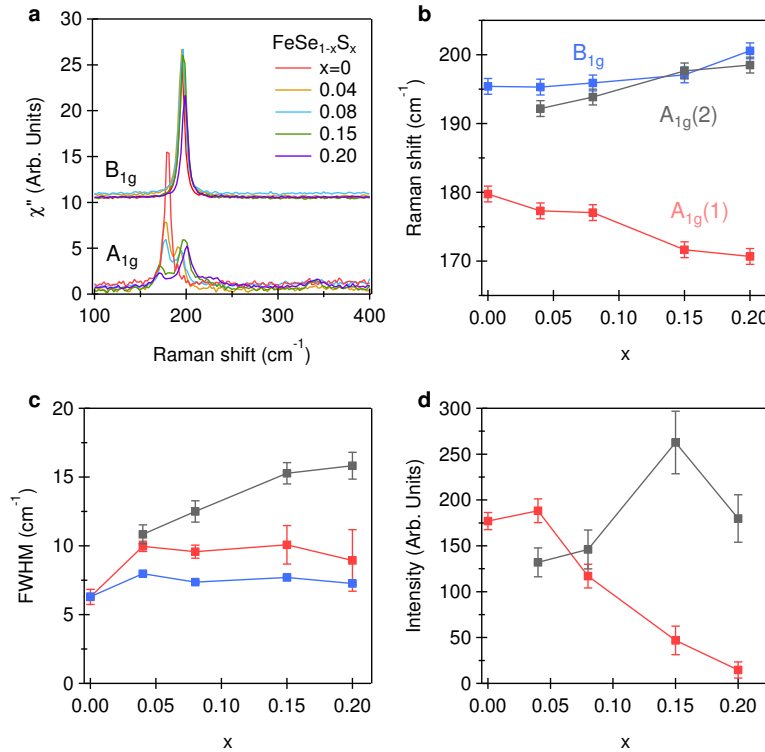


FIG. 7. (a) A_{1g} and B_{1g} symmetry phonon spectra at room temperature. The B_{1g} spectra are offset in the vertical direction. (b-c) Doping dependence of the energy and line width of the B_{1g} and two A_{1g} phonons. (c) The integrated intensity of the two A_{1g} phonons. Error bars in (b) are determined by the instrument energy resolution 2.3 cm^{-1} . Error bars in (c) and (d) are the fitting standard errors.

Origin of the XY symmetry electronic continuum

An intense electronic Raman continuum in the XY-symmetry channel is a common feature for most FeSC materials. For $\text{FeSe}_{1-x}\text{S}_x$ the spectra can be decomposed into two main features (see Fig. 9): (i) A Drude-like low-energy quasi-elastic scattering peak (QEP); and (ii) A broad electronic continuum. The intensity of the QEP is weak at high temperatures, its intensity increases while the maximum of the peak's frequency decreases upon cooling to T_S . The intensity of continuum also increases with cooling, but the enhancement is much milder than for the QEP.

The QEP in the FeSC has been associated with Pomeranchuk-like electronic nematic fluctuations arising from degeneracy of the partially filled iron $3d_{xz}$ and $3d_{yz}$ orbitals [53–55]. The QEP is caused by dynamical charge oscillations in sub-THz frequency range, which give rise to fluctuating charge ferro-quadrupole moment with an amplitude proportional to the locally oscillating charge imbalance $n_{xz} - n_{yz}$ [38].

If the quadrupole moments oscillate in phase, they often show critical behavior leading to a d -wave Pomeranchuk instability at $q = 0$ [38, 56]. These ferro-quadrupole fluctuations most dramatically manifest themselves in the low-frequency part of XY-symmetry Raman response as the Drude-like overdamped quasi-elastic feature in the normal state [5, 34, 38] which undergoes a metamorphosis into a coherent in-gap collective mode below T_c [38–40, 57, 58]. In the orthorhombic phase, the four-fold rotation symmetry on the Fe site is broken and hence the degeneracy of Fe $3d_{xz}$ and $3d_{yz}$ is lifted, which cause rapid suppression of the low-energy quadrupole fluctuations.

However, if the quadrupole moments on the neighboring iron sites prefer to oscillate in opposite phase, it may lead to $q=(\pm\pi,\pm\pi)$ stripe-quadrupole order with broken translational symmetry, see Fig. 10. In such case the broad

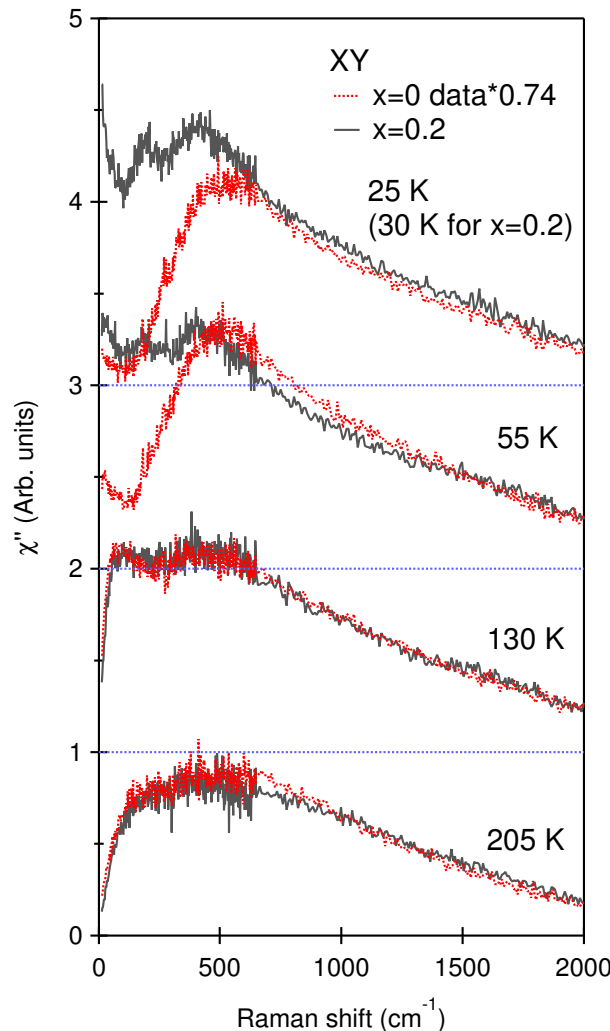


FIG. 8. Temperature evolution of XY symmetry Raman response for FeSe and $\text{FeSe}_{0.8}\text{S}_{0.2}$. The spectra are offset for clarity.

Raman continuum in the high temperature phase arises from a pair of stripe quadrupole excitations at $q=(\pi,\pi)$ and $-q=(-\pi,-\pi)$. A gap opens up in the spectra of quadrupole excitations in the low temperature phase, when the translational symmetry is broken.

Data Fit

We fit the data above T_S with

$$\chi''(\omega, T > T_S) = \chi''_{QEP}(\omega, T) + \chi''_C(\omega, T), \quad (1)$$

Below T_S , $\chi''(\omega, T)$ is fitted with

$$\chi''(\omega, T < T_S) = \chi''_{QEP}(\omega, T) + \chi''_C(\omega, T)\Theta(\omega, T) \quad (2)$$

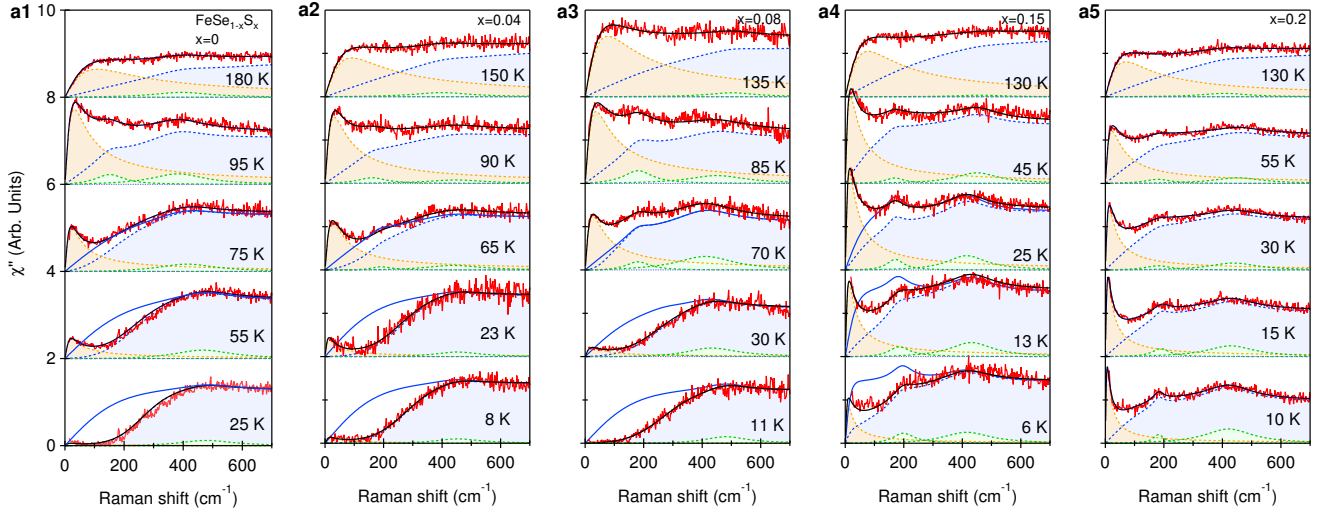


FIG. 9. $\chi''(\omega, T)$ (red) at representative temperatures and the fitting results with the decompositions of the QEP χ''_{QEP} (orange shade) and the continuum $\chi''_C \times \Theta$ (blue shade). The two Lorentz oscillators χ''_L at around 190 and 450 cm^{-1} are shown in green shade. For $x \leq 0.15$, in the low-temperature phase, the gapless continuum χ''_C are shown in blue solid curves.

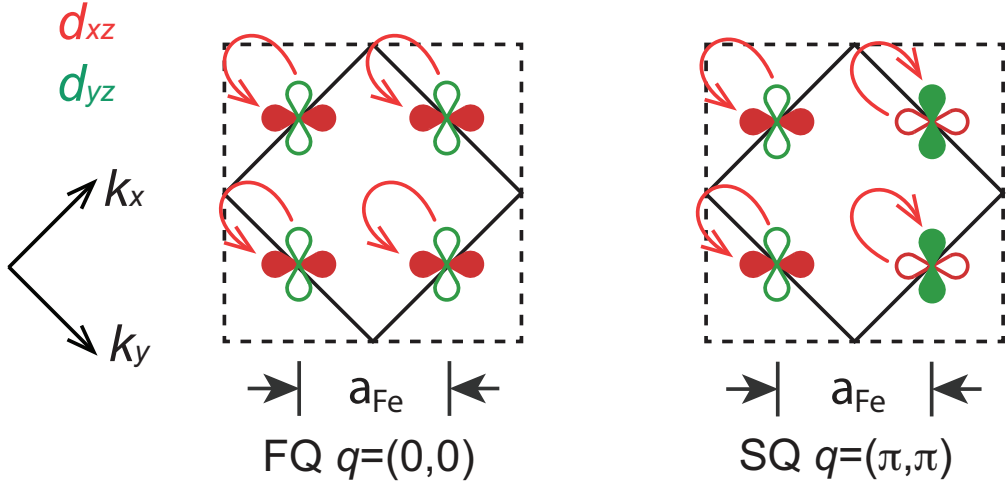


FIG. 10. Illustration of ferro-quadrupole fluctuations and stripe-type quadrupole fluctuations that give rise to the QEP and the broad continuum in XY symmetry Raman response.

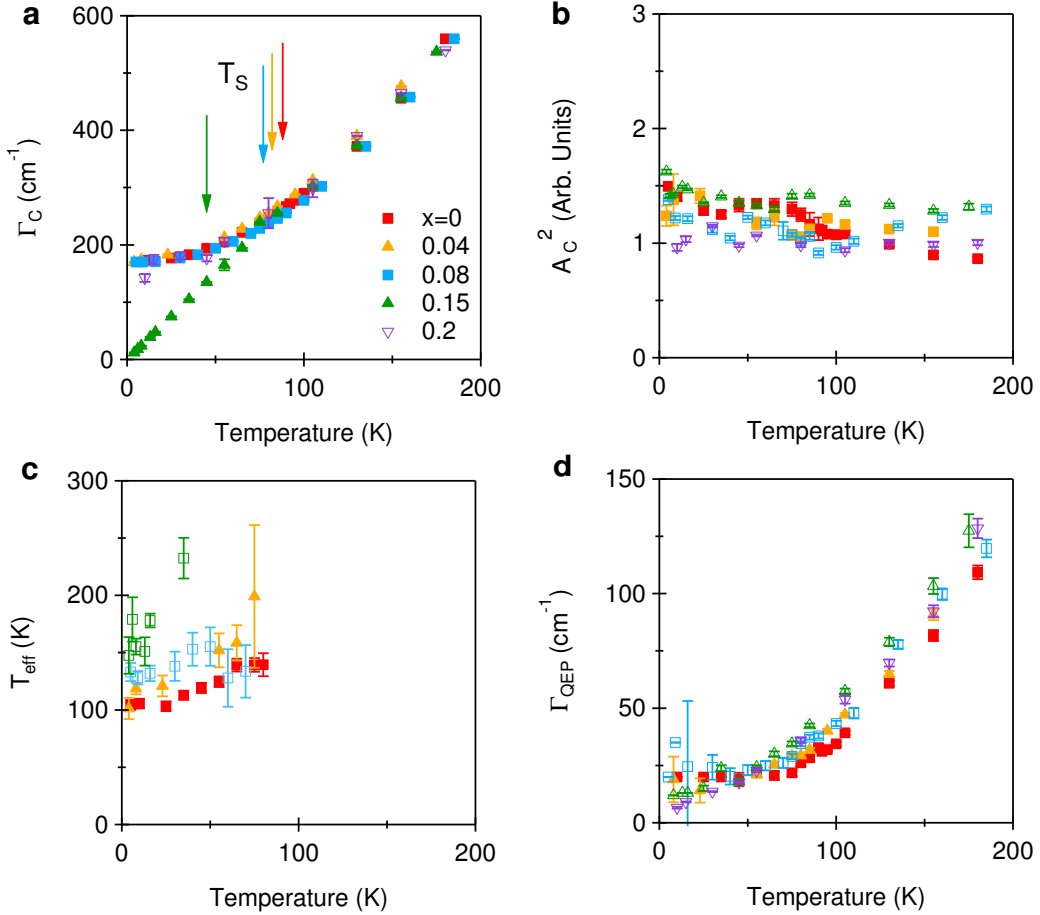


FIG. 11. Fitting parameters as a function of temperature and sulfur content. Error bars are the fitting standard errors.

Here

$$\chi''_{QEP}(\omega, T) = A_{QEP}^2(T) \frac{\omega \Gamma_{QEP}(T)}{\omega^2 + \Gamma_{QEP}^2(T)}, \quad (3)$$

$$\chi''_C(\omega, T) = A_C^2(T) \tanh[\omega/\Gamma_C(T)] + \chi''_L(\omega, T), \quad (4)$$

$$\chi''_L(\omega, T) = A_L^2 \left[\frac{1}{[\omega - \omega_L(T)]^2 + \Gamma_L^2(T)} - \frac{1}{[\omega + \omega_L(T)]^2 + \Gamma_L^2(T)} \right], \quad (5)$$

and

$$\Theta(\omega, T) = \frac{1}{2} \left(1 + \tanh \left[\frac{\omega - 2\Delta(T)}{2k_B T_{eff}} \right] \right). \quad (6)$$

We collect the fitting parameters in Fig. 11. $\Gamma_C(T)$ exhibits a quadratic temperature dependence for all sulfur concentrations $\Gamma_C = 170 + 0.012T^2$ except for $x = 0.15$, for which a linear extrapolation $\Gamma_C = 3T$ gives the best result (see Fig. 11a). The latter is likely due to the vicinity of the nematic quantum critical point as it was reported in Ref. [20].

A_C is almost invariant of T and x (Fig. 11b). T_{eff} for the nematic gap decreases with lowering temperature and always is higher than the real temperature (Fig. 11c). Γ_{QEP} is a linear function of temperature for at $T > T_S$. For $x \leq 0.15$ samples, on entering into the nematic state, Γ_{QEP} deviates from the linear temperature dependence and saturates at about 20 cm^{-1} at low temperatures. In contrast, for the $x = 0.2$ sample, Γ_{QEP} continues to decrease linearly with cooling (Fig. 11d).

All the Raman response data $\chi''(\omega, T)$ and the fitting functions from Eq. 1 are collected in Fig. 9.

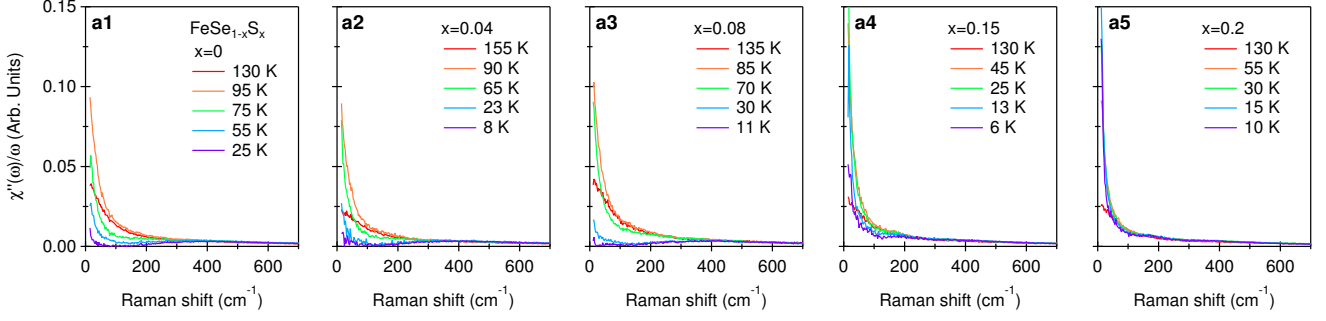


FIG. 12. $\chi''(\omega, T)$ at selected temperatures for $x = 0, 0.04, 0.08, 0.15$ and 0.2 .

Static susceptibility

The real part of the Raman susceptibility $\chi'(\omega)$ can be derived from the imaginary part $\chi''(\omega)$ by Kramers-Kronig transformation. We calculate the static susceptibility $\chi(0)$ by

$$\chi(0) = \frac{2}{\pi} P \int_0^{\omega_1} \frac{\chi''(\omega)}{\omega} d\omega, \quad (7)$$

where ω_1 is a high-energy cut-off. For the QEP that has a Drude form (Eq. 4), $\chi_{QEP}(0) = A_{QEP}^2$ could be derived from the analytical function. We perform a numerical integration to calculate $\chi_C(0, T)$. As shown in Fig. 12, $\chi''(\omega)/\omega$ for $\omega > 500 \text{ cm}^{-1}$ is small and independent of temperature, therefore we choose a high-energy cut-off $\omega_1 = 500 \text{ cm}^{-1}$. For the response function below the low-energy measurement limit, we use a linear extrapolation determined from the fitting parameter of $\chi''_C(\omega, T)$.

Response in the superconducting phase

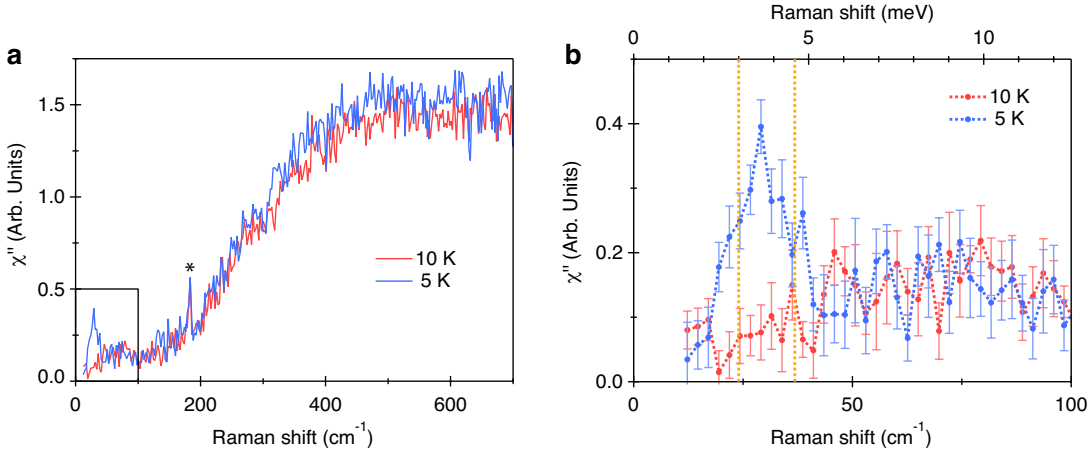


FIG. 13. (a) XY symmetry Raman response in FeSe at 10 K (normal state) and 5 K (superconducting state). (b) Zoom in of the spectra in (a). The error bars are calculated from the standard deviation. The magnitudes of the superconducting gaps $2\Delta_{SC} = 3$ and 4.6 meV defined by the scanning tunneling spectroscopy [16] are shown by vertical dotted lines. The mode at 183.5 cm^{-1} marked with an asterisk in Fig. 13a is the A_g symmetry phonon mode. The phonon intensity appears in the XY scattering geometry because the A_{1g} and B_{2g} symmetry channels merge when the high-temperature D_{4h} group is reduced to the low-temperature D_{2h} group [59].

In Fig. 13 we show the XY symmetry Raman response at 10 K (normal state) and 5 K (superconducting state). In the superconducting state, the quasi-elastic scattering (QEP) is completely suppressed and a sharp symmetric peak at 29 cm^{-1} (3.6 meV) appears. The mode energy is between the two superconducting gap values $2\Delta_{SC} = 3$ and 4.6

meV, as the gaps are determined by tunneling spectroscopy [16]. Therefore, we relate the mode to nematic resonance that appears in the superconducting state when the critical damping for the dynamical Pomeranchuk-like fluctuations is removed [36–40].

* wz131@physics.rutgers.edu

† On leave from Beijing National Laboratory for Condensed Matter Physics and Institute of Physics, Chinese Academy of Sciences, Beijing, 100190, China

‡ girsh@physics.rutgers.edu

- [1] E. Fradkin, S. A. Kivelson, M. J. Lawler, J. P. Eisenstein, and A. P. Mackenzie, *Annu. Rev. Condens. Matter Phys.* **1**, 153 (2010).
- [2] G. R. Stewart, *Science* **83**, 1589 (2011).
- [3] J. Paglione and R. L. Greene, *Nat Phys* **6**, 645 (2010).
- [4] R. M. Fernandes, A. V. Chubukov, and J. Schmalian, *Nat. Phys.* **10**, 97 (2014).
- [5] Y. Gallais, R. M. Fernandes, I. Paul, L. Chauvière, Y.-X. Yang, M.-A. Méasson, M. Cazayous, A. Sacuto, D. Colson, and A. Forget, *Phys. Rev. Lett.* **111**, 267001 (2013).
- [6] A. E. Bohmer, P. Burger, F. Hardy, T. Wolf, P. Schweiss, R. Fromknecht, M. Reinecker, W. Schranz, and C. Meingast, *Phys. Rev. Lett.* **112**, 047001 (2014).
- [7] J.-H. Chu, H.-H. Kuo, J. G. Analytis, and I. R. Fisher, *Science* **337**, 710 (2012).
- [8] X. Lu, J. T. Park, R. Zhang, H. Luo, A. H. Nevidomskyy, Q. Si, and P. Dai, *Science* **345**, 657 (2014).
- [9] S.-H. Baek, D. V. Efremov, J. M. Ok, J. S. Kim, J. van den Brink, and B. Büchner, *Nat Mater* (2014).
- [10] A. E. Böhmer and C. Meingast, *Comptes Rendus Physique* , (2015).
- [11] A. V. Chubukov, M. Khodas, and R. M. Fernandes, *Phys. Rev. X* **6**, 041045 (2016).
- [12] Y. Gallais and I. Paul, *Comptes Rendus Physique* **17**, 113 (2016).
- [13] A. P. Dioguardi, T. Kissikov, C. H. Lin, K. R. Shirer, M. M. Lawson, H.-J. Grafe, J.-H. Chu, I. R. Fisher, R. M. Fernandes, and N. J. Curro, *Phys. Rev. Lett.* **116**, 107202 (2016).
- [14] Y. Schattner, S. Lederer, S. A. Kivelson, and E. Berg, *Phys. Rev. X* **6**, 031028 (2016).
- [15] L. Classen, R.-Q. Xing, M. Khodas, and A. V. Chubukov, *Phys. Rev. Lett.* **118**, 037001 (2017), and refs therein.
- [16] P. O. Sprau, A. Kostin, A. Kreisel, A. E. Böhmer, V. Taufour, P. C. Canfield, S. Mukherjee, P. J. Hirschfeld, B. M. Andersen, and J. C. S. Davis, *Science* **357**, 75 (2017).
- [17] See Supplemental Material at [url put by publisher] for details of data analysis, phonons and the spectra in the superconducting state, which includes Refs. [53–59].
- [18] T. M. McQueen, A. J. Williams, P. W. Stephens, J. Tao, Y. Zhu, V. Ksenofontov, F. Casper, C. Felser, and R. J. Cava, *Phys. Rev. Lett.* **103**, 057002 (2009).
- [19] A. E. Böhmer, T. Arai, F. Hardy, T. Hattori, T. Iye, T. Wolf, H. v. Löhneysen, K. Ishida, and C. Meingast, *Phys. Rev. Lett.* **114**, 027001 (2015).
- [20] S. Hosoi, K. Matsuura, K. Ishida, H. Wang, Y. Mizukami, T. Watashige, S. Kasahara, Y. Matsuda, and T. Shibauchi, *Proc. Natl. Acad. Sci. USA* **113**, 8139 (2016).
- [21] M. A. Tanatar, A. E. Böhmer, E. I. Timmons, M. Schütt, G. Drachuck, V. Taufour, K. Kothapalli, A. Kreyssig, S. L. Bud'ko, P. C. Canfield, R. M. Fernandes, and R. Prozorov, *Phys. Rev. Lett.* **117**, 127001 (2016).
- [22] P. Massat, D. Farina, I. Paul, S. Karlsson, P. Strobel, P. Toulemonde, M.-A. Masson, M. Cazayous, A. Sacuto, S. Kasahara, T. Shibauchi, Y. Matsuda, and Y. Gallais, *Proc. Natl. Acad. Sci. USA* **113**, 9177 (2016).
- [23] A. Baum, H. N. Ruiz, N. Lazarević, Y. Wang, T. Böhm, R. Hosseiniyan Ahangharnejhad, P. Adelmann, T. Wolf, Z. V. Popović, B. Moritz, T. P. Devereaux, and R. Hackl, ArXiv e-prints (2017), arXiv:1709.08998.
- [24] M. D. Watson, T. K. Kim, L. C. Rhodes, M. Eschrig, M. Hoesch, A. A. Haghimirad, and A. I. Coldea, *Phys. Rev. B* **94**, 201107 (2016).
- [25] A. I. Coldea and M. D. Watson, *Annu. Rev. Condens. Matter Phys.* **9**, 125 (2018).
- [26] A. Fedorov, A. Yaresko, T. K. Kim, Y. Kushnirenko, E. Haubold, T. Wolf, M. Hoesch, A. Grüneis, B. Büchner, and S. V. Borisenko, *Sci. Rep.* **6**, 36834 (2016).
- [27] H. C. Xu, X. H. Niu, D. F. Xu, J. Jiang, Q. Yao, Q. Y. Chen, Q. Song, M. Abdel-Hafiez, D. A. Chareev, A. N. Vasiliev, Q. S. Wang, H. L. Wo, J. Zhao, R. Peng, and D. L. Feng, *Phys. Rev. Lett.* **117**, 157003 (2016).
- [28] T. Hanaguri, K. Iwaya, Y. Kohsaka, T. Machida, T. Watashige, S. Kasahara, T. Shibauchi, and Y. Matsuda, ArXiv e-prints (2017), arXiv:1710.02276.
- [29] W. Qing-Yan, L. Zhi, Z. Wen-Hao, Z. Zuo-Cheng, Z. Jin-Song, L. Wei, D. Hao, O. Yun-Bo, D. Peng, C. Kai, W. Jing, S. Can-Li, H. Ke, J. Jin-Feng, J. Shuai-Hua, W. Ya-Yu, W. Li-Li, C. Xi, M. Xu-Cun, and X. Qi-Kun, *Chin. Phys. Lett.* **29**, 037402 (2012).
- [30] J.-F. Ge, Z.-L. Liu, C. Liu, C.-L. Gao, D. Qian, Q.-K. Xue, Y. Liu, and J.-F. Jia, *Nat Mater* **14**, 285 (2015).
- [31] D.-H. Lee, *Science* **357**, 32 (2017).
- [32] K. Matsuura, Y. Mizukami, Y. Arai, Y. Sugimura, N. Maejima, A. Machida, T. Watanuki, T. Fukuda, T. Yajima, Z. Hiroi, K. Y. Yip, Y. C. Chan, Q. Niu, S. Hosoi, K. Ishida, K. Mukasa, T. Watashige, S. Kasahara, J.-G. Cheng, S. K. Goh, Y. Matsuda, Y. Uwatoko, and T. Shibauchi, (2017), arXiv:1704.02057.

- [33] V. Gnezdilov, Y. G. Pashkevich, P. Lemmens, D. Wulferding, T. Shevtsova, A. Gusev, D. Chareev, and A. Vasiliev, *Phys. Rev. B* **87**, 144508 (2013).
- [34] F. Kretzschmar, T. Bohm, U. Karahasanovic, B. Muschler, A. Baum, D. Jost, J. Schmalian, S. Caprara, M. Grilli, C. Di Castro, J. G. Analytis, J. H. Chu, I. R. Fisher, and R. Hackl, *Nat. Phys.* **12**, 560 (2016).
- [35] Q. Wang, Y. Shen, B. Pan, Y. Hao, M. Ma, F. Zhou, P. Steffens, K. Schmalzl, T. R. Forrest, M. Abdel-Hafiez, X. Chen, D. A. Chareev, A. N. Vasiliev, P. Bourges, Y. Sidis, H. Cao, and J. Zhao, *Nat. Mater.* **15**, 159 (2016).
- [36] F. Kretzschmar, B. Muschler, T. Böhm, A. Baum, R. Hackl, H.-H. Wen, V. Tsurkan, J. Deisenhofer, and A. Loidl, *Phys. Rev. Lett.* **110**, 187002 (2013).
- [37] A. Hinojosa, J. Cai, and A. V. Chubukov, *Phys. Rev. B* **93**, 075106 (2016).
- [38] V. K. Thorsmølle, M. Khodas, Z. P. Yin, C. Zhang, S. V. Carr, P. Dai, and G. Blumberg, *Phys. Rev. B* **93**, 054515 (2016).
- [39] Y. Gallais, I. Paul, L. Chauvière, and J. Schmalian, *Phys. Rev. Lett.* **116**, 017001 (2016).
- [40] S.-F. Wu, P. Richard, H. Ding, H.-H. Wen, G. Tan, M. Wang, C. Zhang, P. Dai, and G. Blumberg, *Phys. Rev. B* **95**, 085125 (2017).
- [41] This is in contrast to interpretations in Ref. [22, 23], where authors claimed a relation between the 450 cm^{-1} peak to nematicity, see [17] for details.
- [42] W.-L. Zhang, P. Richard, H. Ding, A. S. Sefat, J. Gillett, S. E. Sebastian, M. Khodas, and G. Blumberg, ArXiv e-prints (2014), [arXiv:1410.6452](https://arxiv.org/abs/1410.6452).
- [43] C.-C. Lee, W.-G. Yin, and W. Ku, *Phys. Rev. Lett.* **103**, 267001 (2009).
- [44] W. Lv, J. Wu, and P. Phillips, *Phys. Rev. B* **80**, 224506 (2009).
- [45] T. Saito, S. Onari, and H. Kontani, *Phys. Rev. B* **82**, 144510 (2010).
- [46] H. Yamase and R. Zeyher, *Phys. Rev. B* **88**, 125120 (2013).
- [47] H. Kontani and Y. Yamakawa, *Phys. Rev. Lett.* **113**, 047001 (2014).
- [48] R.-Q. Xing, L. Classen, M. Khodas, and A. V. Chubukov, *Phys. Rev. B* **95**, 085108 (2017).
- [49] R. Yu and Q. Si, *Phys. Rev. Lett.* **115**, 116401 (2015).
- [50] Q. Wang, Y. Shen, B. Pan, X. Zhang, K. Ikeuchi, K. Iida, A. D. Christianson, H. C. Walker, D. T. Adroja, M. Abdel-Hafiez, X. Chen, D. A. Chareev, A. N. Vasiliev, and J. Zhao, *Nat. Commun.* **7**, 12182 (2016).
- [51] A. Kreisel, B. M. Andersen, P. O. Sprau, A. Kostin, J. C. S. Davis, and P. J. Hirschfeld, *Phys. Rev. B* **95**, 174504 (2017).
- [52] P. Zhang, X.-L. Peng, T. Qian, P. Richard, X. Shi, J.-Z. Ma, B. B. Fu, Y.-L. Guo, Z. Q. Han, S. C. Wang, L. L. Wang, Q.-K. Xue, J. P. Hu, Y.-J. Sun, and H. Ding, *Phys. Rev. B* **94**, 104510 (2016).
- [53] V. Cvetkovic and O. Vafek, *Phys. Rev. B* **88**, 134510 (2013).
- [54] J. Hu and N. Hao, *Phys. Rev. X* **2**, 021009 (2012).
- [55] W.-L. Zhang, W. R. Meier, T. Kong, P. C. Canfield, and G. Blumberg, ArXiv e-prints (2018), [arXiv:1804.06963](https://arxiv.org/abs/1804.06963).
- [56] Y. A. Pomeranchuk, Sov. Phys. JETP **8**, 361 (1958).
- [57] M. Khodas, A. V. Chubukov, and G. Blumberg, *Phys. Rev. B* **89**, 245134 (2014).
- [58] S. Maiti, A. V. Chubukov, and P. J. Hirschfeld, *Phys. Rev. B* **96**, 014503 (2017).
- [59] S.-F. Wu, W.-L. Zhang, L. Li, H.-B. Cao, H.-H. Kung, A. S. Sefat, H. Ding, P. Richard, and G. Blumberg, ArXiv e-prints (2017), [arXiv:1712.01903](https://arxiv.org/abs/1712.01903).